Surrogate based Multidisciplinary Design Optimization of a VTOL aircraft

Catarina João Fonseca Ribeiro
catarina.fonseca.ribeiro@tecnico.ulisboa.pt

Instituto Superior Técnico, Universidade de Lisboa, Portugal

May 2021

Abstract

This work aims at evaluating surrogate based Multidisciplinary Design Optimization (MDO) strategies for designing an Urban Air Mobility (UAM) Vertical Take-Off and Landing (VTOL) aircraft. During the conceptual stages, it is important to have a vast exploration of the design space, using models for several disciplines that need to be considered regarding the mission requirements. Surrogate models are a potentially good approach to rapidly explore the design space. Therefore, in this work, a comparison between the results of a MDO using real functions and the surrogate models of these functions is provided. Three major strategies for the aircraft optimization are carried out: an optimization using the real, analytical functions and their derivatives with the adjoint method; a surrogate-based optimization where surrogate models for both the objective function and constraints are built, using the Surrogate Modeling Toolbox (SMT); and an optimization based on adaptive sampling and infill criteria such as the Watson and Barnes criterion (WB2). To compare these MDO strategies, an energy minimization problem is established for the VTOL aircraft as a case study in OpenMDAO, where aerodynamics and structures are modeled using the low-fidelity models provided in the OpenAeroStruct (OAS) framework. Initially, only two design variables are considered. Then, more design variables are added to the problem, and therefore increasing the complexity of the optimization problem.

Keywords: Multidisciplinary design optimization, surrogate models, adaptive sampling, aircraft design, aerostructural design

1. Introduction

Over the last years, there has been a significant increase in the research of Urban Air Mobility (UAM), with the number of applications also growing [1]. New problems have to be solved in order to turn UAM into a reality, as the society also demands a cleaner and more sustainable aviation, capable of responding to the requisites of transportation in urban scenarios. As these demands grow, the necessity for developing tools that consider different requirements from different disciplines also increases. Hence, Multidisciplinary Analysis and Optimization (MDAO) [2] is a tool that can be very useful in early stages of designing a new aircraft, where usually there is a great exploration of possible concepts. Using MDAO allows a designer to integrate multiple disciplines, for example aerodynamics, structures, propulsion, emissions, performance, among others, with the objective of considering the influence of a discipline on the others, so that in the end, the obtained solution is one that satisfies a compromise between all the disciplines taken into account. As the complexity of the problem increases, by the increment in disciplines considered, or the higher fidelity models used, the computational burden of this optimization can become too demanding.

One possible approach to solve this problem is by the use of surrogate models, that try to mimic the the real functions [3].

This work aims at comparing three optimization strategies, used to solve an aircraft design problem: (i) optimization using the real functions with sensitivities computed by means of the adjoint method; (ii) optimization using the surrogate models of the previous functions; (iii) optimization using adaptive sampling with the WB2 criterion [4]. The aircraft design problem consists in minimizing the energy consumption of a Vertical Take-Off and Landing (VTOL) aircraft for UAM. The physical models are defined using a low-fidelity tool, the OpenAeroStruct (OAS) [5] and the optimization problem is defined using the OpenMDAO framework [6]. The surrogate models are built using the open-source Surrogate Modeling Toolbox (SMT) [7].

2. Background

2.1. Surrogate models

A surrogate model is an approximation model that tries to mimic the behaviour of the real model [3]. This model is cheaper to evaluate than the original one. To build such a model there are three main steps: (i) set a Design of Experiments (DOE) to obtain a set of sample points, in this case the Latin Hypercube Sampling (LHS) [3] is used, and choose a modeling technique; (ii) evaluate the real functions at the given points and train the model; (iii) test and validate the surrogate model built. The chosen model in this work is the Kriging model, which assumes that a deterministic response can be estimated by $\hat{y}(x) = f(x) + Z(x)$, where $f(x)$ is a regression model and $Z(x)$ is a random process [7]. The regression model used in this work is assumed to be a constant unknown, $\mu_m(x)$. A Gaussian process is used for the random part of the Kriging model, with zero mean and a covariance defined

by:

$$cov[Z(x), Z(x')] = \sigma^2 R(x, x') \tag{1}$$

where x and x' are two points in the design space, σ^2 is the process variance and $R(x, x')$ is the spatial correlation, *i.e.* the kernel function. The most common kernel function, and the one used on this work, is the squared exponential kernel function, given by:

$$R(x, x') = \sum_{l=1}^{d} \exp(-\theta_l (x_l - x'_l)^2) \tag{2}$$

where each $\theta_l \in \mathbb{R}$ is a hyperparameter, and there are d hyperparameters, with d being the number of design variables.

The mean of the Gaussian process, μ_m, and the process variance, σ^2, can be estimated by maximizing the likelihood function and with these two estimated, a prediction for the function being modeled can be done by:

$$\hat{y}(x) = \hat{\mu}_m + \{\psi\}^T [\Psi]^{-1} (\{y\} - \{1\}\hat{\mu}_m) \tag{3}$$

where $\{\psi\}$ is the vector of correlations between the sampled data and the new prediction, $[\Psi]$ is the correlation matrix for the sampled data, $\{y\}$ is the real function values of the sample points and $\{1\}$ is a $n \times 1$ column vector of ones. It is also possible to estimate the variance of the prediction made with:

$$\hat{s}^2(x) = \hat{\sigma}^2 \left[1 - \{\psi\}^T [\Psi]^{-1} \{\psi\} + \frac{1 - \{1\}^T [\Psi]^{-1} \{\psi\}}{\{1\}^T [\Psi]^{-1} \{1\}} \right] \tag{4}$$

2.2. Infill criteria

The surrogate models are trained based on a set of sample points, as explained before. However, an adaptive sampling may be used, *i.e.*, a sampling plan which is updated by adding points in some areas of interest. These new points are chosen according to the criterion defined. The Expected Improvement (EI) [8] is a criterion that balances exploration of the design space and exploitation, and its calculated using the information provided by the Kriging model:

$$E[I(x)] = (y_{min} - \hat{y}(x))\Phi\left(\frac{y_{min} - \hat{y}(x)}{\hat{s}(x)}\right) + \hat{s}(x)\phi\left(\frac{y_{min} - \hat{y}(x)}{\hat{s}(x)}\right) \tag{5}$$

where $\Phi(\cdot)$ is the cumulative distribution function, $\phi(\cdot)$ is the probability density function of the standard normal distribution and y_{min} is the minimum value of the sample data values. It should be noted, that in equation (5), when $\hat{s}(x) = 0$ then $E[I(x)] = 0$. The point to be added to the sample is the one that maximizes the EI function. This function is a multi-modal function, that can be costly to evaluate when used in an optimization process. Therefore, the Watson and Barnes criterion was proposed [9]. This criterion smooths the EI criterion, by using the prediction of the Kriging model:

$$WB2(x) = \hat{y}(x) - E[I(x)] \tag{6}$$

2.3. Multidisciplinary Design Analysis and Optimization

2.3.1 Framework architecture and solver

The architecture sets the structure of how the Multidisciplinary Design Analysis and Optimization (MDAO) problem is going to be solved, it defines the sequence of the optimization [2]. In this work, a Multi-Discipline Feasible (MDF) [2] architecture is used, which ensures that in each iteration the two disciplines used, aerodynamics and structures, are coupled. The eXtended Design Structure Matrix (XDSM) diagram [10] of this architecture is depicted in Figure 1.

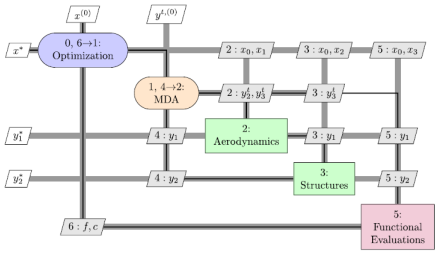

Figure 1: XDSM of a MDF architecture using a Gauss-Seidel solver [5].

In each iteration of the optimization, each discipline analysis is done and the Multidisciplinary Design Analysis (MDA) solver ensures the convergence between the different disciplines (aerodynamics and structures). After, the objective function and constraints are calculated with the variables that result from the MDA and the point to be evaluated at the next iteration is defined. In this work, the MDA solver used is a Non-Linear Block Gauss-Seidel (NLBGS) approach with Aitken relaxation.

2.3.2 Aerodynamic model

The aerodynamic model used is the one implemented on OAS [5], which is the Vortex Lattice Method (VLM) [11]. This method uses a series of lifting lines instead of just one, with the wing being discretized along the span and along the chord leading to lifting panels. Each of these is represented by a single horseshoe vortex of constant unknown strength at a given control point. The bound vortex is located at the quarter-chord of each panel and the control point's location is at the center line of the panel (in the spanwise direction) and at three quarter-chords from the front. At each control point, the vortices induce a velocity, $\overrightarrow{V}$, that can be calculated by using the Biot-Savart law [11]:

$$d\overrightarrow{V} = \frac{\Gamma}{4\pi} \frac{d\overrightarrow{l} \times \overrightarrow{r}}{||\overrightarrow{V}||^3} \tag{7}$$

where $\overrightarrow{V}$ is the induced flow velocity, Γ is the circulation of the considered vortex, $d\overrightarrow{l}$ a finite length of the vortex filament and $\overrightarrow{r}$ is the position of the control point relative to the filament. By combining all the vortex circulations, Γ, using the superposition method, the induced velocity at each control point u_n can then be calculated:

$$u_n = \sum_{j=1}^{N} A_{i,j} \Gamma_j \tag{8}$$

where N is the number of vortices, *i.e.* the number of panels and $A_{i,j}$ is a row of the aerodynamic influence coefficient matrix, which represents the influence of the vortex on panel j on the induced velocity of panel i.

Since the method used, the VLM, assumes an incompressible potential flow, some corrections are made so that the values of the drag and lift coefficients are more accurate. A compressible correction is made to the pressure coefficient, C_p, by using the Prandtl-Glauert theory [11]:

$$C_p = \frac{C_{p,0}}{\sqrt{1 - \mathrm{M}_\infty^2}} \tag{9}$$

where $C_{p,0}$ is the linearised pressure coefficient for the incompressible flow and M_∞ is the Mach number of the undisturbed flow.

A viscous correction is also applied to correct the drag coefficient, based on the skin friction of a flat-plate, both under laminar and turbulent flow. This calculated skin-friction drag is then adjusted to take into account the pressure drag using a form factor for lifting surfaces, presented in [12].

2.3.3 Structural model

A Finite Element Method (FEM) [13] is employed, by using a spatial beam element of two nodes, each with six degrees of freedom, which assembles two bending elements, a torsion element and an axial element [5].

The local stiffness matrices are calculated, and then the global stiffness matrix $[K]$ is assembled by transforming the local matrices to the global frame. The loads applied to the structure are calculated by the aerodynamic model, and therefore the displacement vector can now be calculated [13], using :

$$[K]\{u\} = \{F\} \tag{10}$$

where $\{F\}$ is the load vector, and $\{u\}$ is the unknown displacement vector.

To determine if the structure fails under the applied load, the Von-Mises equivalent stress [13] is calculated and compared with the admissible load, using a safety factor of 1.5.

2.3.4 Fluid-Structure Interaction

During the multidisciplinary analysis, information from one discipline is passed to the other and so there is a need to define a Fluid Structure Interaction (FSI) algorithm. Knowing the aerodynamic and structural solution is already known at iteration k, the coupled solution at iteration k + 1 can be obtained by first solving the aerodynamic system for the current iteration, then integrating the aerodynamic loads onto the structural domain, followed by the structural analysis with the aerodynamic loads as input. After the displacement transfer from the structural analysis to the aerodynamic surface mesh is done and finally the mesh is updated and the aerodynamic system is solved again and everything is repeated until convergence is achieved.

After this the MDA is done, and the objective function and constraints are calculated, as mentioned before.

2.3.5 Optimization algorithms

To determine the next point to be evaluated at each iteration, different algorithms can be used. These can be classified into deterministic, which are then divided into gradient-based and gradient-free, or heuristic [14]. In this work, a gradient-based and a heuristic algorithms are used.

A gradient-based algorithm uses information from both the objective function value and also its derivatives with respect to the design variables, to compute the search direction and consequently the next point to be considered in the optimization. In this work, the gradient-based algorithm chosen is the Sequential Least-Square Quadratic Programming (SLSQP) [15]. The adjoint method [14] is used to provide the gradients when using the real functions.

An heuristic algorithm tries to mimic some natural behaviour and use a certain amount of randomness to avoid getting trapped at a local optimum. The algorithm used in this case is the Genetic Algorithm (GA) [16], which is based on natural evolution.

3. Implementation

The sequence of the aircraft design optimization problem developed during this work can be summarized with the flowchart presented in Figure 2.

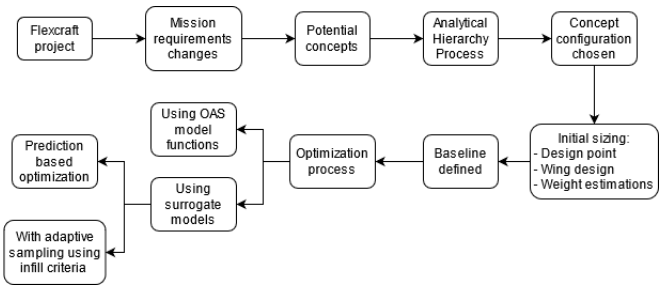

Figure 2: Implementation process flowchart

Firstly, the Flexcraft project [17] concept and the changes in the mission are analysed, and some potential concepts to be used for the new mission are studied. The best concept is chosen by using an Analytical Hierarchy Process (AHP) [18] and then an initial sizing is done. This initial sizing is performed by using design point equations, analysing stability conditions to define a baseline for the wing, and every components' weight and position are estimated so that the centre of gravity of the new concept can be calculated. This way, a baseline for the optimization is set. Then the optimization process starts, using the OpenMDAO framework [6], and it can be done either using the real OAS model functions, or using the surrogate models. The latter also presents two possible ways, and so the surrogate-based optimization can occur using the surrogate model itself (prediction-based) or using infill criteria functions.

3.1. Conceptual design

An initial conceptual design is performed according to the new mission profile, so that a baseline for the optimization can be defined.

3.1.1 Choice of the configuration

First, an AHP is performed to choose the configuration to be used. The criteria chosen to perform this study are:

- Aerodynamics - When assuming a constant weight, specific fuel consumption, velocity and range, the fuel

consumption decreases with the increase of the aerodynamic efficiency, L/D.

- Weight and Structures - The concept should be a result of a compromise between structural stiffness and robustness and its weight.
- Propulsion - The propulsive system efficiency has to be taken into account as it has a large impact on the fuel and battery consumption.
- Manufacturing and Maintenance - The more complex the aircraft's systems are, the more expensive its maintenance and manufacturing will be. For example the maintenance costs depend on the number of engines and electric motors, increasing the expenses as the level of complexity grows.
- Stability and Control - Given that the mission does not require high manoeuvrability, the stability of the concept is favoured. The control during the VTOL parts of the mission also impacts the decision making process on the initial concept.
- Take-off and Landing capabilities - The regulations for this kind of vehicle here considered are not well developed yet. Based on regulations for general aviation, an evaluation on the capabilities to take-off and particularly land in critical conditions (such as motor inoperative) were taken into consideration.
- Noise - Since the goal is to design an unmanned aerial vehicle with VTOL capacity to be used in regional connections between urban centres, the noise produced by the system (especially during the mission phase inside cities) has also an impact on the choice of the concept.

Five concepts were analysed with this process. The configuration of each concept can be observed in Figure 3. After carrying out the AHP, concept I is chosen.

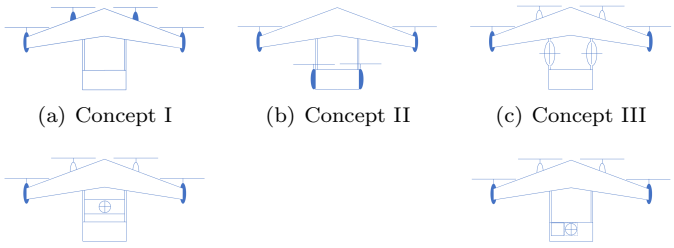

(a) Concept I (b) Concept II (c) Concept III

(d) Concept IV (e) Concept V

Figure 3: Configurations analysed during the conceptual design phase. The rotors that with a solid colour have tilting capability.

3.1.2 Design point

Having chosen a concept for the general configuration of the aircraft and using the MTOM of 3500 kg of the Flexcraft project, now some general dimensions can be defined. This is done using the design point equations, for both vertical and forward flight. A more detailed explanation of the design point analysis can be found in [12].

First, the forward flight is considered, where the Wing Loading and the Power Loading that satisfy all the mission requirements are estimated. The Wing Loading is W/S and Power Loading is W/P, where W is the aircraft's weight, S is the wing area, and P is the required power. The wing loading affects some parameters of aircraft performance, such as the stall speed or range, and so it has to be chosen according to the mission requirements. The conditions considered are the stall speed, the maximum wing loading for range, and the maximum power loading for both a defined climb angle and for cruise. With these four conditions, the design space can be plotted (see Figure 4) and the design point found. This is the point where the cruise line intersects the stall condition, since it is the one that maximizes both power loading and wing loading.

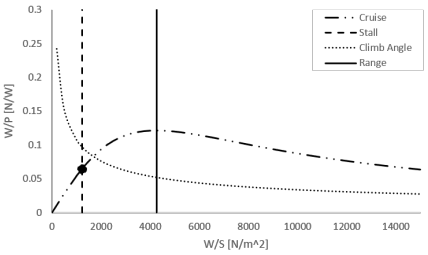

Figure 4: Design space and design point for the forward flight

Now, the vertical flight conditions are considered, where the Power Loading and the Disc Loading need to satisfy once again the mission requirements, with the disc loading being W/A_R, where A_R is the total rotor area. Once again, four conditions are considered: the maximum disc loading, $DL_{max} = 600\ \mathrm{N\,m^{-2}}$, which is a typical value for a tilt rotor [19] and the maximum power loading for vertical climb, hover and transition.

As it was done before for the forward flight phase, now the design space can be plotted, as shown in Figure 5. The dot corresponding to the intersection between the vertical climb condition and the maximum disc loading represents the design point.

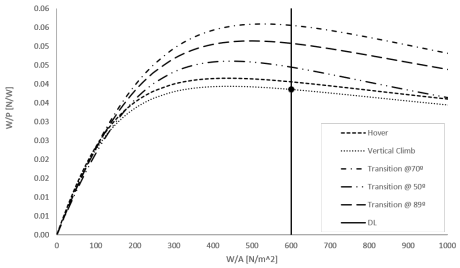

Figure 5: Design space and design point for the vertical flight

Combining the two design points, an initial sizing of the aircraft is done and the results are presented in Table 1.

Table 1: Initial sizing based on the design point considerations

$\left(\frac{W}{P}\right)_{ff}$	$\left(\frac{W}{S}\right)$	$\left(\frac{W}{P}\right)_{vf}$	$\left(\frac{W}{A}\right)$	W	P_{ff}	P_{vf}	S	A_R
$[\mathrm{N\,W^{-1}}]$	$[\mathrm{N\,m^{-2}}]$	$[\mathrm{N\,W^{-1}}]$	$[\mathrm{N\,m^{-2}}]$	[N]	[kW]	[kW]	$[\mathrm{m^2}]$	$[\mathrm{m^2}]$
0.0641	1218	0.0386	600	34335	535	890	28.18	57.23

3.1.3 Weight and balance estimations

Initially, for the design points considerations, the mass of the aircraft was assumed to be the same as in the Flexcraft project, 3500 kg. However, to estimate the center of gravity (CG) position, some predictions of each component's weight and locations have to be made. The estimations for the weight of each component were done by using empirical equations, presented in both [12] and [20], or by using some previous estimations done for the Flexcraft project. The position of each component was also estimated, based on the configuration chosen and some values of the Flexcraft project. The final total mass was estimated in 3529.74 kg, a value close to the one from Flexcraft project.

3.1.4 Wing initial design

The airfoil used was kept the same as the one on the Flexcraft project and the same happens for the horizontal stabilizer airfoil. However, since the mission has changed, the wing planform is now different from the one on the original concept. The wing span and the taper ratio were kept the same, but the wing tip and root chord are now different, because the obtained wing area is also different. Also, the wing sweep angle has to change because of the longitudinal static stability. A study was made to evaluate the static margin of the aircraft using different sweep angles. The results are presented in Figure 6.

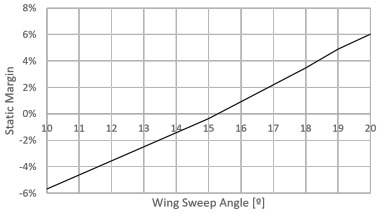

Figure 6: Static margin variation with the wing sweep angle

The wing for the baseline is therefore characterized by the parameters shown in Table 2. The horizontal stabilizer was not modified, being the same as the one from the Flexcraft project (see Table 3).

Table 2: Wing dimensions

Parameter	Nomenclature	Value	Units
Span	b	15	m
Mean aerodynamic chord	$\bar{c}$	1.994	m
Root chord	c_{root}	2.684	m
Tip chord	c_{tip}	1.074	m
Taper ratio	TR	0.4	–
Sweep	Λ	20	°
Dihedral	Γ_d	2	°

3.1.5 Propulsive system architecture

Even though a detailed study on the propulsive systems is out of the scope of this work, a brief description of the general architecture of the system is here provided.

The propulsive system consists in an hybrid series configuration, shown in Figure 7. In this configuration, the internal combustion engine burns fuel and rotates an AC generator. The power generated can be used to charge the batteries and to be delivered to the AC electric motors that drive the propellers. The series configuration allows for a separation of power and thrust generation and also to have different flight modes, i.e, to have flight phases where only the electric energy of the batteries is used to propel the aircraft, and other phases where only the Internal Combustion Engine (ICE) is the provider of the necessary energy. This way, the vertical climb, hover, transition and vertical descent are driven using the batteries and the forward flight phases are carried out using only fuel energy. Therefore, the ICE and generator can be sized for only cruise, which allows the system to be working at a steady state in most of the mission, and so it is working with the same specific fuel consumption (SFC), at the optimal engine point. However, this system implies an increase of the propulsive system weight and its complexity.

Table 3: Horizontal stabilizer dimensions

Parameter	Nomenclature	Value	Units
Span	b	4	m
Root chord	c_{root}	1.86	m
Taper ratio	TR	1	–
Sweep	Λ	0	°
Dihedral	Γ_d	0	°

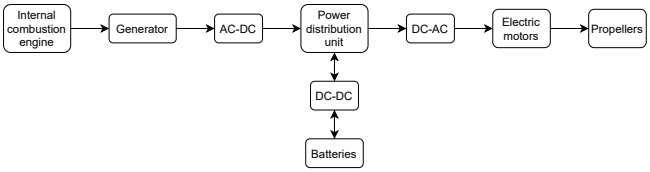

Figure 7: Propulsive system high-level representation

3.2. Optimization problem formulation

Using the mission requirements, the optimization is formulated by defining the objective function, the design variables and the constraints. The main requirements for the mission considered are: (i) a cruise speed of 110 $\mathrm{m\,s^{-1}}$; (ii) a fixed range of 800 km; (iii) a payload of 500 kg; (iv) a static margin between 5 % and 20 % and an ability to have a trimmed flight; (v) structural integrity in both the VTOL phases and a pull-up manoeuvre of 3.8g.

3.2.1 Objective function

With the range fixed, one main objective is to minimize the fuel consumption. Also, since VTOL phases play a major role in the power required, which influences the weight of the rotors and batteries, this power should also be considered. In order to deal with these different possible objectives, an energetic objective function is used, combining the energy spent during both cruise and VTOL operations. This way the total energy is given by:

$$E = m_{fuel} \times E_{spec_{fuel}} + P_{vc} \times t_{vc} + P_{hover} \times t_{hover} + E_{tr} \tag{11}$$

where m_{fuel} is the mass of necessary fuel to complete the cruise phase, calculated with the Breguet equation; $E_{spec_{fuel}}$ is the fuel's specific energy density, assumed to be equal to 43.28 $\mathrm{MJ\,kg^{-1}}$; P_{vc} and P_{hover} is the power

needed for the vertical climb and hover phases, respectively, which are calculated using the design point equations; t_{vc} and t_{hover} are the times of the vertical climb and hover phases, respectively; and E_{tr} is the energy needed for the transition phase, which is assumed to be constant.

3.2.2 Design variables

Different case studies are made, using different design variables (DV). Here all the DV used are presented. The wing planform is defined using a linear distribution for the chord, by controlling the chord at the root, $(c_{root})_{wing}$, and the chord at the tip $(c_{tip})_{wing}$. The same happens for the horizontal tail planform, using $(c_{root})_{tail}$ and $(c_{tip})_{tail}$. The wingbox structure is defined by the thickness of the spars and the skins. Using the OAS model for the wingbox, the rear and front spar thicknesses, $(t_{spar})_{wing}$, are considered to be the same, as well as the upper and lower skin thicknesses, $(t_{skin})_{wing}$. A constant thickness is considered along the span for both the spars and the skins. This consideration was taken because of manufacturing restrictions. Once again, the same happens for the horizontal tail, thus adding two more design variables, $(t_{spar})_{tail}$ and $(t_{skin})_{tail}$. The angle of attack at cruise condition, α, is also used as design variable in one of the case studies.

3.2.3 Constraints

To ensure a longitudinally stable aircraft, the static margin [12], K_n, will have to be between 5 and 20 % as mentioned before. Directional and lateral stability are not considered on this thesis, since the vertical stabilizers are not being considered to the optimization problem, and are assumed to be equal to the ones on the Flexcraft project. Additionally, in order to have a trimmed flight during cruise, a constraint regarding the pitching moment coefficient, C_M, is used, and is also imposed that lift must be equal to the total weight. During the pull-up manoeuvre considered, an additional constraint is imposed, so that the lift is equal to the total weight multiplying by the pull up load factor, $n = 3.8g$. Two load cases are considered: the vertical climb, and a pull-up of 3.8g. The four critical points on the wingbox, explained in [21], must satisfy the structural failure criterion at these ultimate load cases. The criterion used is the Von-Mises failure criterion. Finally, a constraint regarding the volume of the necessary fuel is employed. This, ensures that the volume occupied by the fuel is smaller than the available volume inside the wingbox structure of the wing.

The constraints' equations were arranged in a manner that to be satisfied they need to be negative (apart from the fuel volume constraint, which needs to be positive). Since there are computational errors and limitations, each equality constraints was transformed into two inequality constraints.

3.3. Optimization cycle

Before building the surrogate models, and solving the optimization problem using these approximated functions, the problem is solved using the real functions and their analytical derivatives. Summarily, the optimization cycle when using the real functions is described by the flowchart of Figure 8.

In the approach where the surrogate models are used, the objective function of the optimization problem is the surrogate model itself, without adding any additional sample points. As shown in Figure 9, firstly the DOE is generated and the surrogate models, for the objective functions and every constraint, are built. Having the new, approximated, functions, the optimization problem is then solved using the SLSQP algorithm. The final solution is then evaluated with the real model to check if there are any major discrepancies.

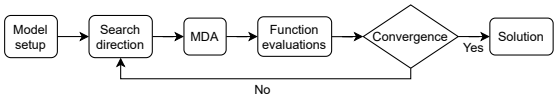

Figure 8: Optimization cycle when using the real functions

Figure 9: Optimization cycle when using the surrogate models

On the other hand, in the adaptive sampling approach, instead of using the objective function surrogate model as the function to be minimized, an infill criterion function is used instead. The constraints used in the problem correspond to the constraints' surrogate models.

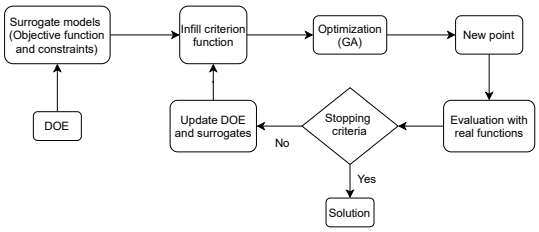

Figure 10: Optimization cycle when using the adaptive sampling approach

As shown in Figure 10, an initial DOE is generated and the initial surrogate models are built. After this, the infill criterion function is defined, using the objective function (total energy) surrogate model. At this point, the objective function, for the optimizer to minimize, becomes the infill criterion function itself. The optimization problem is solved using a genetic algorithm, and the solution obtained is then evaluated with the real model and a new sample point is added to the DOE. The surrogate models, and consequently the infill criterion. function, are then updated and the process starts over again until convergence is achieved.

4. Results

4.1. Baseline and Case studies

The baseline is defined according to the studies done in the conceptual design phase, as explained before. The wing and horizontal tail planform are already defined, and shown in Tables 2 and 3. The baseline wing spar and skin thicknesses are both equal to 0.0038 m, and the horizontal tail spar and skin thicknesses are equal to 0.00255 m. The angle of attack used for the baseline is equal to $-0.8°$. The presented configuration is evaluated using the OAS framework and its performance parameters are shown in Table 4.

Table 4: Baseline performance

Wing structural mass [kg]	Horizontal tail structural mass [kg]	Fuel [kg]	Total mass [kg]	L/D	Total energy [MJ]
408.35	37.68	407.07	3524.10	13.36	17937.11

Several case studies of the problem are carried out, each using different design variables in the optimization. The design variables used in each case study done are presented in Table 5.

Table 5: Design variables used in each case study

Case study	Attitude	Wing				Tail			
	α	c_{root}	c_{tip}	t_{spar}	t_{skin}	c_{root}	c_{tip}	t_{spar}	t_{skin}
2.1		x			x				
2.2			x	x					
2.3	x	x							
4		x	x	x	x				
8		x	x	x	x	x	x	x	x

4.2. Surrogate model's accuracy

Before carrying out the optimization, using the three different approaches explained before, a study on the surrogate models' accuracy for each case is done. The goal is to find out how many points are needed to have a surrogate model that is able to correctly mimic the real function behaviour. Both the objective function and each constraints' surrogate models are tested using a different set of test points for each case. Only the results of the average relative error of the objective function, the total energy, are presented here.

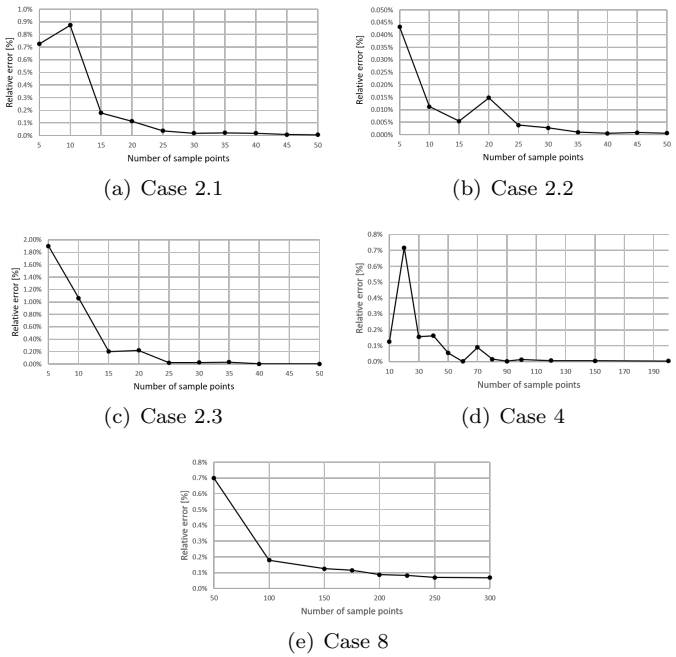

(a) Case 2.1

(b) Case 2.2

(c) Case 2.3

(d) Case 4

(e) Case 8

Figure 11: Average relative error of the objective function surrogate model for each case

The objective function surrogate model in each case presents very low values of the average relative error even with a small number of sample points. However there are some constraints that show a significantly higher relative error (sometimes around 300%). In the cases where this happens, these constraints show a non-linear behaviour, which explains the need to have more sample points so that the surrogates can capture the real behaviour of the function. Even so, with an increase of the number of sample points, the relative error tends to decrease and converge to a value near 0%.

The number of sample points needed to have a relative error smaller than 5% is: 35 for case study 2.1; 10 for case 2.2; 25 for case 2.3; 40 for case 4 and more than 300 for case 8.

4.3. Optimization results

For each case study, the optimization problem is solved using three different approaches previously mentioned: (i) using the real functions, implemented on OAS and using the adjoint method; (ii) using the surrogate models of these real functions; (iii) using an adaptive sampling with the WB2 criterion. For the first two strategies, the optimization algorithm is the SLSQP, while for the last approach the GA is used instead.

4.3.1 Case 2.1

The results for case 2.1 obtained with the three strategies mentioned before are presented in Table 6.

Table 6: Results of the different solutions of case 2.1

	Wing root chord [m]	Wing skin thickness [m]	Wing structural mass [kg]	Fuel [kg]	Total mass [kg]	L/D	Total energy [MJ]
Baseline	2.684	0.0038	408.35	407.07	3524.10	13.36	17937.11
Real functions	2.739	0.00155	228.68 -44.00 %	378.10 -7.12 %	3315.47 -5.92 %	13.54 1.35 %	16433.35 -8.38 %
Surrogate search	2.739	0.00154	228.26 -44.10 %	378.02 -7.14 %	3314.96 -5.93 %	13.54 1.38 %	16429.71 -8.40 %
Adaptive sampling	2.739	0.00157	230.06 -43.66 %	378.42 -7.04 %	3317.16 -5.87 %	13.54 1.38 %	16446.95 -8.31 %

All the three solutions present similar results, with differences between them smaller than 1%. This way the results obtained with the surrogate models are validated. It is worth to notice that the performance parameters, that correspond to strategies where the surrogate models are used, are the real function evaluations when those design variables.

In the second approach, the optimization results shown correspond to the ones when the surrogate models are built using 50 sample points. When the adaptive sampling is used, the starting sampling plans to build the surrogate models are composed by: 5 sample points in the case of the objective function, 20 sample points for the constraints with a linear behaviour, and 50 sample points for the constraints with non-linear behaviour. In this last approach, the number of individuals for each population and the number of generations used by the GA are 200 and 100, respectively. The number of points added to the sampling plans is 50. However, the best solution is found after the third iteration, *i.e.* after adding three points.

In terms of computational cost, the number of iterations, function and gradient evaluations associated with each approach are presented in Table 7.

The benefits of using the surrogate models, in terms of computational cost (Table 7), are not verified in this case, since the optimization using the real functions when using the SLSQP algorithm with the gradient information

Table 7: Computational cost of the four methods for case 2.1

	Real functions (SLSQP)	Surrogate search	Adaptive sampling
Iterations	6	11	50
Function evaluations	6	44 (+50)	1000000 (+50+50)
Gradient evaluations	6	11	0

obtained from the adjoint method takes only 6 iterations to find the optimum, which corresponds to 6 function and gradient evaluations. On the other hand, the second approach takes 44 surrogate model predictions and 50 real function evaluations to build the surrogate models, while the adaptive sampling approach takes 10^5 surrogate model predictions plus 100 real functions evaluations (50 to build the initial surrogate models and one for each of the 50 points added).

4.3.2 Case 2.2

The different solutions obtained in this case are presented in Table 8.

Table 8: Results of the different solutions of Case 2.2

	Wing tip chord [m]	Wing spar thickness [m]	Wing structural mass [kg]	Fuel [kg]	Total mass [kg]	L/D	Total Energy [MJ]
Baseline	1.074	0.0038	408.35	412.76	3529.79	13.19	17937.11
Real functions	1.340	0.00108	363.58 -10.96 %	397.75 -3.64 %	3470.01 -1.69 %	13.47 2.18 %	17286.07 -3.63 %
Surrogate search	1.347	0.00100	362.06 -11.34 %	397.39 -3.73 %	3468.13 -1.75 %	13.48 2.20 %	17270.45 -3.72 %
Adaptive sampling	1.341	0.00111	364.38 -10.77 %	397.76 -3.63 %	3470.82 -1.67 %	13.47 2.18 %	17286.72 -3.63 %

The results from the different approaches are, once again, very similar to each other, with differences smaller than 1%.

The results correspondent to the surrogate search approach are obtained when using 10 sample points to build the surrogate models. With the adaptive sampling approach, the number of sample points of the starting sampling plan is: 5 for the total energy and 20 for the constraints. Once again, in this approach the GA is used and the number of individuals and the number of generations used are 200 and 100, respectively. Since in the previous case, the 50 points added turned out to be excessive, because it was noted that the number of repeated points was very high, in this case only 25 points were added to the sampling plans.

In terms of computational cost, a comparison between the different approaches is presented in Table 9.

Table 9: Computational cost of the different approaches for Case 2.2

	Real functions	Surrogate search	Adaptive sampling
Iterations	8	3	25
Function evaluations	10	4 (+10)	500000 (+20+25)
Gradient evaluations	8	3	0

Similarly to the previous case, the optimization with the real functions presents the smallest computational cost, having only 10 real functions' evaluations, while the optimization using the surrogate models need only 4 surrogate model predictions but it also needs 10 real functions evaluations to build models. The adaptive sampling approach is the most costly, needing $50 \cdot 10^4$ surrogate model predictions, plus 20 real function evaluations to build the total energy and the constraints initial surrogate models, plus the 25 real functions evaluations (one for each added point). In this case, the computational cost of the first two approaches is very similar since the real functions optimization takes 10 real function evaluations, which is the same value needed to build the surrogate models, and it takes only 4 more surrogate models predictions in the second approach.

4.3.3 Case 2.3

The different solutions obtained with the used approaches are presented in Table 10.

Table 10: Results of the different solutions of Case 2.3

	Wing root chord [m]	Angle of attack [°]	Wing structural mass [kg]	Fuel [kg]	Total mass [kg]	L/D	Total energy [MJ]
Baseline	2.684	-0.8	408.35	407.07	3524.10	13.36	17937.11
Real functions	2.500	-0.455	388.29 -4.91 %	360.28 -11.49 %	3457.25 -1.90 %	14,91 11.59 %	15664.39 -12.67 %
Surrogate search	2.500	-0.454	388.29 -4.91 %	360.23 -11.51 %	3457.20 -1.90 %	14.91 11.61 %	15662.03 -12.68 %
Adaptive sampling	2.512	-0.465	389.57 -4.60 %	361.54 -11.18 %	3459.79 -1.82 %	14.87 11.30 %	15719.06 -12.37 %

The results are, once more, very consistent between each other, with differences smaller than 1% again. The number of sample points, used to build the surrogate models that lead to the optimal solution in the second approach, is 10. On the other hand, the number of sample points used to build the initial sampling plans in the last approach are: 5 for the total energy function, 25 for every constraint except the pitching moment coefficient, and 40 for this latter constraint. The GA parameters are the same as in case 2.2 and the number of added points found with the WB2 criterion is again 25.

Again, in terms of computational costs (shown in Table 11), the real functions optimization presents a lower number of real function evaluations, 4, while the surrogate based optimization needs only 3 iterations, but it takes 4 surrogate models predictions and 10 real functions evaluations to build the surrogate models. As for the adaptive sampling it takes $50 \cdot 10^4$ surrogate models predictions to find the minimum, plus 40 real functions evaluations to build the initial sampling plans, plus 25 real functions evaluations, one for each added point.

Table 11: Computational cost of the three methods for case 2.3

	Real functions	Surrogate search	Adaptive sampling
Iterations	4	3	25
Function evaluations	4	4 (+10)	500000 (+40+25)
Gradient evaluations	4	3	0

4.3.4 Case 4

The three solutions obtained with each optimization approach are presented in Table 12.

In the second approach, the optimization problem was again solved using the different number of sample points, and the best solution was found when this number is 50. When using the last strategy, the number of starting sam-

Table 12: Results of the different solutions obtained in case study 4

	Tip chord [m]	Root chord [m]	Spar thickness [m]	Skin thickness [m]	Wing structural mass [kg]	Fuel [kg]	Total mass [kg]	L/D	Total energy [MJ]
Baseline	1.074	2.684	0.0038	0.0038	408.35	407.07	3524.10	13.36	17937.11
Real functions	0.972	2.812	0.00196	0.00171	191.99 -52.98 %	375.72 -7.70 %	3275.66 -7.05 %	13.46 0.75 %	16329.59 -7.69 %
Surrogate search	0.982	2.818	0.00155	0.00186	194.64 -52.33 %	376.78 -7.44 %	3280.10 -6.92 %	13.44 0.60 %	16375.18 -7.43 %
Adaptive sampling	0.959	2.825	0.00245	0.00178	210.41 -48.47 %	378.99 -6.90 %	3298.08 -6.41 %	13.43 0.52 %	16471.23 -6.89 %

ple points are: 10 for the total energy functions, 30 for every constraint except two of the failure criteria of the wing in the pull-up manoeuvre, in which case the number of samples is 40. Again, the GA was used in this approach, using a number of individuals of 300 and a number of generations of 100. The number of added points to the sampling plans is 50. In this case, contrarily to what happened in the two DV cases, the 50 points added show different results in almost every iterations, which suggests that not enough points were added, and a better solution could still be found. Also, the number of unfeasible points added increased, which shows that there are still some errors in the surrogate models, even though their accuracy seems high (average relative error lower than 3%).

The differences between the different solutions are not very significant (less than 1 %), but the best solution corresponds to the one found when the real functions are used. As stated before, the solution found with the last approach may correspond to a local minimum because the population sizes or the number of generations are smaller than needed, or the number of points added is too low. The small amount of individuals, generations and points added is explained by the time constraints existing. In the approach where the surrogate models are used, and the optimization problem is solved using the SLSQP, the optimizer may got trapped in a local minimum as well, since, even though the starting point is the same as the one used in the real functions approach, the prediction of the derivatives or the functions can show some errors, and so the optimizer is guided to a slightly different solution.

Table 13: Computational cost of the different optimization approaches for case 4

	Real functions	Surrogate search	Adaptive sampling
Iterations	14	21	50
Function evaluations	21	34 (+50)	1500000 (+40+50)
Gradient evaluations	14	17	0

In terms of computational cost, the surrogate models still do not shown an advantage, since the real functions approach takes only 21 real functions evaluations, while the surrogate model approach needs 34 surrogate models' predictions plus 50 real functions evaluations to build the models, and the last approach takes $15 \cdot 10^5$ surrogate models' predictions plus 40 real functions evaluations to build the initial sampling plans plus a real functions evaluation for each of the 50 points added.

4.3.5 Case 8

The values of the design variables of the different solutions found are presented in Table 14, and the corresponding performance parameters, of each solution, are presented in Table 15.

Table 14: Design variables values of the different solutions obtained in case study 8

	Wing tip chord [m]	Wing root chord [m]	Wing spar thickness [m]	Wing skin thickness [m]	Tail tip chord [m]	Tail root chord [m]	Tail spar thickness [m]	Tail skin thickness [m]
Baseline	1.074	2.684	0.0038	0.0038	1.86	1.86	0.00255	0.00255
Real functions	1.230	2.511	0.00199	0.00222	1.15	1.15	0.0005	0.00168
Surrogate search	1.205	2.533	0.0028	0.00203	1.15	1.15	0.0005	0.00089
Adaptive sampling	1.253	2.488	0.00986	0.00132	1.155	1.161	0.00348	0.00054

Table 15: Performance parameters of the different solutions obtained in case study 8

	Wing structural mass [kg]	Horizontal mass structural mass [kg]	Fuel [kg]	Total mass [kg]	L/D	Total energy [MJ]
Baseline	408.35	37.68	407.07	3524.10	13.36	17937.11
Real functions	232.82 -42.99 %	7.85 -79.17 %	349.93 -14.04 %	3261.61 -7.45 %	14.45 8.19 %	15213.01 -14.00 %
Surrogate search	237.67 -41.80 %	7.12 -81.12 %	349.70 -14.09 %	3265.48 -7.34 %	14.48 8.41 %	15203.15 -14.06 %
Adaptive sampling	362.52 -11.22 %	13.14 -65.14 %	362.80 -10.87 %	3409.45 -3.25 %	14.58 9.14 %	15772.57 -10.84 %

The differences between the solutions obtained with the first two approaches are very small. However, the difference of the solution found with the last approach is higher than on the previous cases. This suggests that in the last approach the global minimum was not found. This might have happened because either the number of individuals or the number of added points is too low and so some areas of the design space might not be considered.

In terms of computational cost, the surrogate models present a higher cost once again, with the number of real function evaluations in the first approach being only 15, while in the second approach there are 18 surrogate models predictions plus 200 real functions evaluations to build the sampling plans of the surrogate models, and in the last approach there are $50 \cdot 10^5$ surrogate models predictions, plus 300 real functions evaluations to build the initial sampling plans, plus 200 real functions evaluations, one for each point being added.

Table 16: Computational cost of the different optimization approaches for Case 8

	Real functions	Surrogate search	Adaptive sampling
Iterations	14	19	200
Function evaluations	15	18 (+200)	5000000 (+300+200)
Gradient evaluations	14	18	0

4.4. Optimal solution

The optimal solution found, the one that minimizes the most the total energy needed to complete the defined mission, corresponds to the solution found with the surrogate models in case 8. The proposed configuration presents a wing structural mass that is around 42 % lighter than the wing structural mass of the baseline, a reduction of around 81 % in the horizontal stabilizer structural mass and a reduction of about 14 % of the fuel mass. This leads to an overall mass that is around 7 % smaller than the one of the baseline. The lift-to-drag ratio of this configuration is almost 8.5 % higher than the baseline. The

solution presents a significant reduction of the total energy needed, 14.06 %. The two configurations, the baseline and the optimal solution, are illustrated in Figure 12.

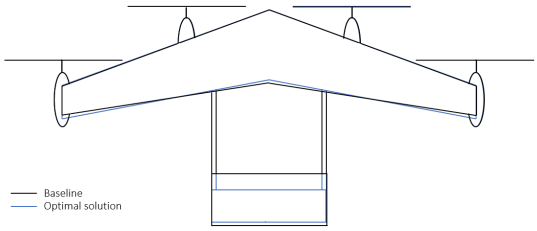

Figure 12: Baseline and optimal solution general configurations

5. Conclusions

When comparing the surrogate models based optimization with the real functions optimization, the latter shows a smaller computational cost, and even though sometimes its solution is slightly worse, it is not very significant. This means, that for the problem at hand, the surrogate models do not present a relevant advantage over the real functions, which are already simple, since the physical models are of low-fidelity.

This can also be explained because the analytical partial derivatives of each function, computed by means of the adjoint method, were possible to give as an input to the optimizer. If for example the derivatives were too complex or not available, the real functions approach may not have been the better strategy.

The design of the wing is also very similar to the baseline used, which can lead to the quick optimization process using the real functions. This can either be happening because the optimization is to constrained, since the number of design variables is relatively small, or because the baseline is already a good design.

References

[1] Suchithra Rajendran et. al. Air taxi service for urban mobility: A critical review of recent developments, future challenges, and opportunities. *Transportation Research Part E: Logistics and Transportation Review*, 143, 2020.

[2] Joaquim R. R. A. et. la. Martins. Multidisciplinary design optimization: A survey of architectures. *AIAA Journal*, 51(9):2049–2075, 2013.

[3] R. Yondo et. al. A review on design of experiments and surrogate models in aircraft real-time and many-query aerodynamic analyses. *Prog. Aerosp. Sci.*, 96:23–61, 2018. doi: 10.1016/j.paerosci.2017.11.003.

[4] M. J. Sasena et. al. Exploration of metamodeling sampling criteria for constrained global optimization. *Engineering Optimization*, 34(3):263–278, 2002.

[5] J. P. Jasa et. al. Open-source coupled aerostructural optimization using python. *Structural and Multidisciplinary Optimization*, 57:1815–1827, 2018.

[6] J. S. Gray et. al. OpenMDAO: An Open-Source Framework for Multidisciplinary Design, Analysis, and Optimization. *Structural and Multidisciplinary Optimization*, 59:1075–1104, 2019.

[7] M. A. Bouhlel et. al. A python surrogate modeling framework with derivatives. *Adv. Eng. Softw.*, 135, 2019. doi: 10.1016/j.advengsoft.2019.03.005.

[8] N. Bartoli et. al. Improvement of efficient global optimization with mixture of experts: methodology developments and preliminary results in aircraft wing design. In *17th AIAA/ISSMO Multidisciplinary Analysis and Optimization Conference*, Washington, DC, USA, 2016.

[9] A. G. Watson et. al. Infill sampling criteria to locate extremes. *Mathematical Geology*, 27(5):589–608, 1995.

[10] A.B. Lambe et. al. Extensions to the design structure matrix for the description of multidisciplinary design, analysis, and optimization processes. *Struct Multidisc Optim*, 46, 2012.

[11] J. D. Anderson. *Fundamentals of Aerodynamics*. McGraw-Hill, 5th edition, 2010.

[12] D. P. Raymer. *Aircraft Design: A Conceptual Approach*. American Institute of Aeronautics and Astronautics, Inc., 4th edition, 2006. ISBN: 1563478293.

[13] J. N. Reddy. *Introduction to the Finite Element Method*. McGraw-Hill Education, 3rd edition, 2006.

[14] J.R.R.A. Martins et. al. *Engineering Design Optimization*. Cambridge University Press (to be published), 2021.

[15] D. Kraft. A Software Package for Sequential Quadratic Programming. Technical Report 28, 1988.

[16] D. E. Goldberg. *Genetic Algorithms in Search, Optimization and Machine Learning*. Addison-Wesley Longman Publishing Co., Inc., USA, 1st edition, 1989.

[17] Flexcraft consortium. FLEXCRAFT - Project's website. https://flexcraft.pt. Accessed on June 2020.

[18] Thomas L. Saaty. *The Analytic Hierarchy Process: Planning, Priority Setting, Resource Allocation*. McGraw-Hil, 1980.

[19] M. D. Maisel et. al. The history of the xv-15 tilt rotor research aircraft: From concept to flight. *NASA SP-2000-4517*.

[20] D. P. Wells et. al. The flight optimization system weights estimation method. *NASA/TM-2017-219627/Volume I*, 2017. https://ntrs.nasa.gov/search.jsp?R=20170005851.

[21] S. S. Chauhan et. al. Low-fidelity aerostructural optimization of aircraft wings with a simplified wingbox model using openaerostruct. In *Proceedings of the 6th International Conference on Engineering Optimization, EngOpt 2018*, Lisbon, Portugal, 2018.